ISSN: 3067-8366
Research Article
Journal of Environmental Science, Sustainability, and Green Innovation

Prediction of Overall Beach Changes on Shizuoka and Shimizu Coasts Using a Morphodynamic (BG) Model

Takaaki Uda[1*], Akinori Sumita[2], Shota Uchiyama[2], & Masaki Murata[3]

[1]*Public Works Research Center, 1-6-4 Taito, Taito, Tokyo 110-0016, Japan*
[2]*Shizuoka Public Work Office, Shizuoka Prefectural Government, 2-20 Ariake, Suruga, Shizuoka City, Shizuoka 422-8031, Japan*
[3]*Coastal Engineering Laboratory, Co., Ltd., 1-22 Wakaba, Shinjuku, Tokyo 160-0011, Japan*

[*]Corresponding author: Takaaki Uda, Public Works Research Center, 1-6-4 Taito, Taito, Tokyo 110-0016, Japan.

Submitted: 14 May 2025 **Accepted:** 21 May 2025 **Published:** 26 May 2025

https://doi.org/10.63620/MKJESSGI.2025.1016

Citation: *Uda, T., Sumita, A., Uchiyama, S., & Murata, M. (2025). Prediction of Overall Beach Changes on Shizuoka and Shimizu Coasts Using a Morphodynamic (BG) Model. J Environ Sci & Sustain & Green Innov, 1(2), 01-15.*

Abstract

Background: *On the Shizuoka and Shimizu coasts located along the western shore of Suruga Bay in Japan, a wide sandy beach had formed owing to the abundant fluvial sand supplied by the Abe River. However, extensive riverbed mining was carried out before the 1970s, resulting in a decrease in sand supply from the river. This caused a significant reduction in longshore sand transport and severe erosion downcoast. As a measure against beach erosion, a large number of detached breakwaters, as well as five artificial headlands, have been constructed along the coastline. Then, after the prohibition of riverbed mining in the 1980s, a large amount of sand was resupplied from the river and such sand was transported alongshore while forming a sand body owing to the existence of detached breakwaters. These movements of the sand body along these coasts were investigated, and measured beach changes were reproduced using the BG model (a model for predicting 3-D beach changes based on Bagnold's concept). By this calculation, we were able to reproduce the overall beach changes of the coast associated with the movement of a sand body, and the effect of beach nourishment was evaluated.*

Keywords: Sand Body, Beach Changes, Shoreline Changes, BG model, Morphodynamic Model, Beach Nourishment, Shizuoka and Shimizu Coasts

Introduction

The Shizuoka and Shimizu coasts located along the western shore of Suruga Bay, Japan, have been formed by the abundant supply of sand from the Abe River that originated from the central mountains (Fig. 1). The southwest and northeast parts of these coasts with respect to the Takigahara River are called the Shizuoka and Shimizu coasts, respectively (Fig. 2). On the Shizuoka coast, the beach was severely eroded owing to the considerable decrease in the amount of fluvial sediment triggered by extensive riverbed mining in the Abe River before 1967. Then, a large number of detached breakwaters were constructed along the coastline as a measure against beach erosion in the 1970's.

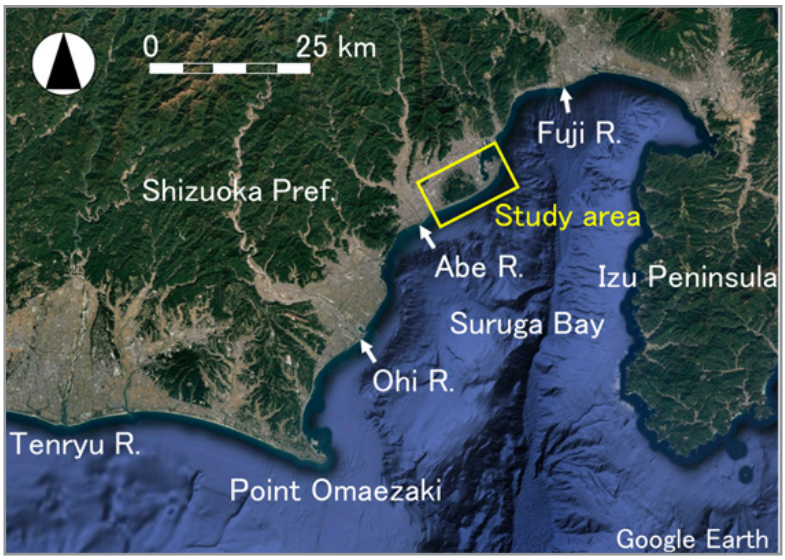

Figure 1: Locations of Abe River and study area.

After the prohibition of riverbed mining in 1967, however, the amount of fluvial sand supplied from the Abe River significantly increased after 1982/1983, resulting in the recovery of sandy beaches near the Abe River mouth [1, 2, 3]. During this process, the northeast end of the sand accumulation zone (sand body) propagated from upcoast to downcoast at a velocity of 260 m/yr, while burying the detached breakwaters. Regarding the movement of the sand body along the Shizuoka coast, [1, 4] reproduced the beach changes associated with the movement of the sand body between 1983 and 2006 using the contour-line-change model under the expanded coordinate system, with which a gradually curving coastline was modeled by a straight coastline. San-nami et al. [5] also calculated beach changes until 2015 using the same model to study the effect of beach nourishment as a method of accelerating the movement of the sand body.

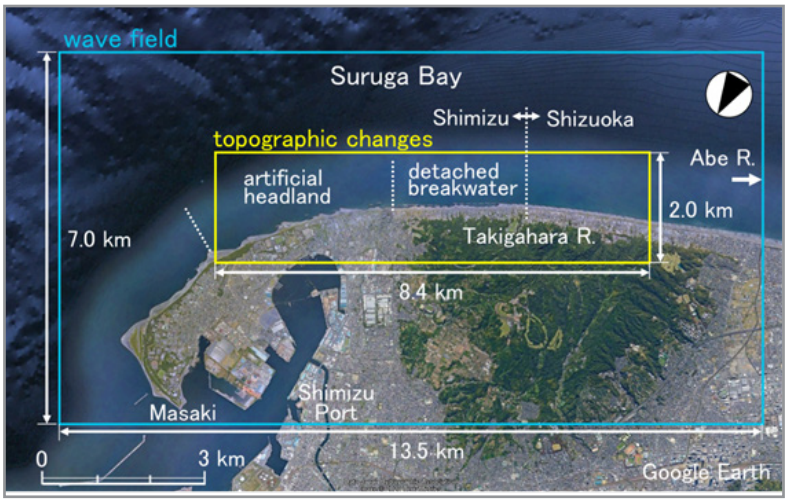

Figure 2: Calculation domain of wave field and topographic changes on Shizuoka and Shimizu coasts.

However, in the analysis of the movement of the sand body using the contour-line-change model, a gradually curving coastline was replaced with a straight coastline using the expanded coordinate system, and the detached breakwaters were also replaced by a straight wall, and thus accurate modeling was inadequate. In addition, on the Shimizu coast, the detached breakwaters with an offshore distance of 50 m different from 90 m on the Shizuoka coast were constructed together with the installation of five artificial headlands (HLs). These differ from the modeled conditions in Uda et al.'s study, and the accurate prediction of the movement of the sand body was difficult. In this study, a real coordinate system was employed, and the topographic changes in the entire area of the Shizuoka and Shimizu coasts associated with the movement of the sand body were reproduced using the BG model (a model for predicting 3-D beach changes using Bagnold's concept) [6, 7]. Then, beach changes over 30 years were predicted, taking into consideration the effect of beach nourishment to enhance the movement velocity of the sand body.

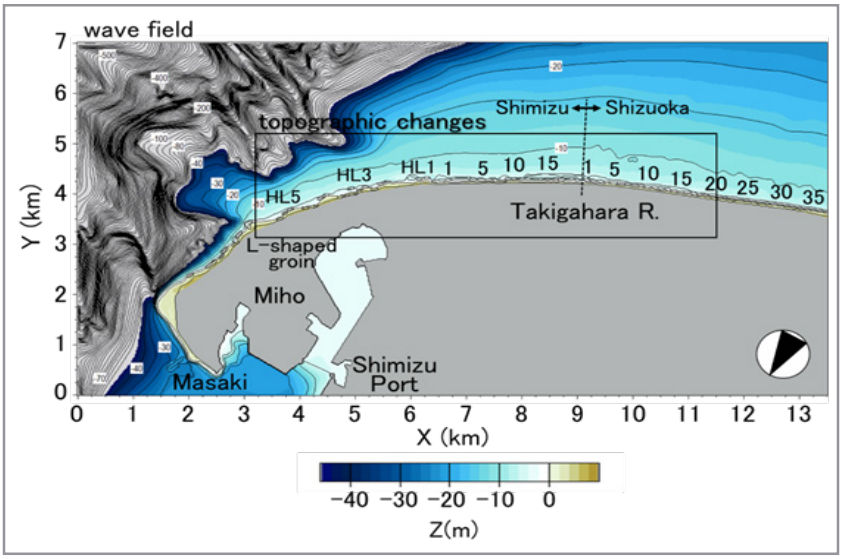

Figure 3: Calculation domains of wave field and topographic changes.

Morphologies of Shizuoka and Shimizu Coasts

The calculation domain of the topographic changes of the Shizuoka and Shimizu coasts is a rectangular area of 13.5 km length alongshore and 7.0 km width in the cross-shore direction, as shown in Fig. 2. In this domain, the orientation of the coastline rotates by an angle of 32° counterclockwise from N71°E near the Oya River mouth to N39°E near the tip of the sand spit with increasing curvature of the coastline in the northeast part. Because waves are primarily incident from the south to these coasts, northeastward longshore sand transport prevails along the coast. Figure 3 shows the bathymetry of the calculation domain for the wave field. Regarding the offshore seabed topography, a continental shelf expands in the longshore direction and its width decreases northeastward with the development of a steep submarine canyon near the east end of the coast. Furthermore, this submarine canyon approaches very close to the shoreline at the north end. North of this area, sand transported northeastward by the longshore sand transport discharges into the submarine canyon via a steep slope around the sand spit. In this study, the north end of the calculation domain was set to the location of an L-shaped groin immediately south of the submarine canyon to investigate the movement of the sand body along the coastline without the offshore discharge of sand via a steep slope.

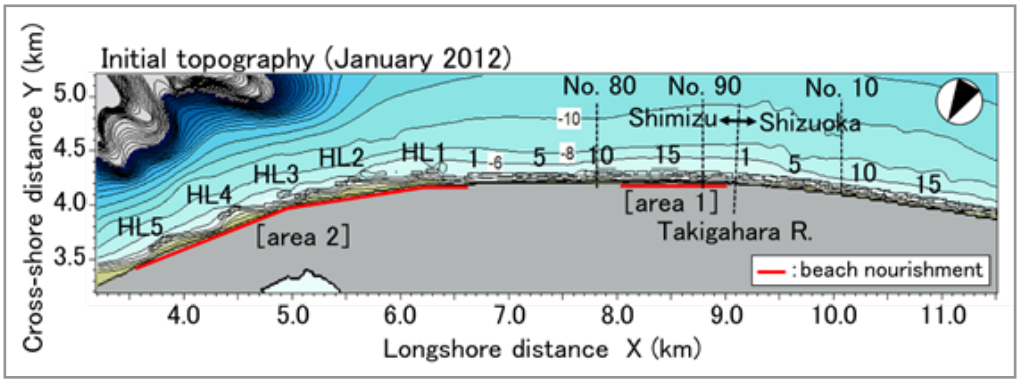

Figure 4: Initial topography (January 2012) and beach nourishment area.

Figure 4 shows the enlargement of the rectangular area in Fig. 3, together with the bathymetry measured in January 2012 and beach nourishment areas. In this area, the beach slope near the shoreline is steep, whereas in the offshore zone, the seabed with a gentle slope extends. Along the Shizuoka coast, detached breakwaters Nos. 1–20 and along the Shimizu coast Nos. 1–19 have been constructed, together with the artificial headland Nos. 1–5 composed of two detached breakwaters along the Shimizu coast.

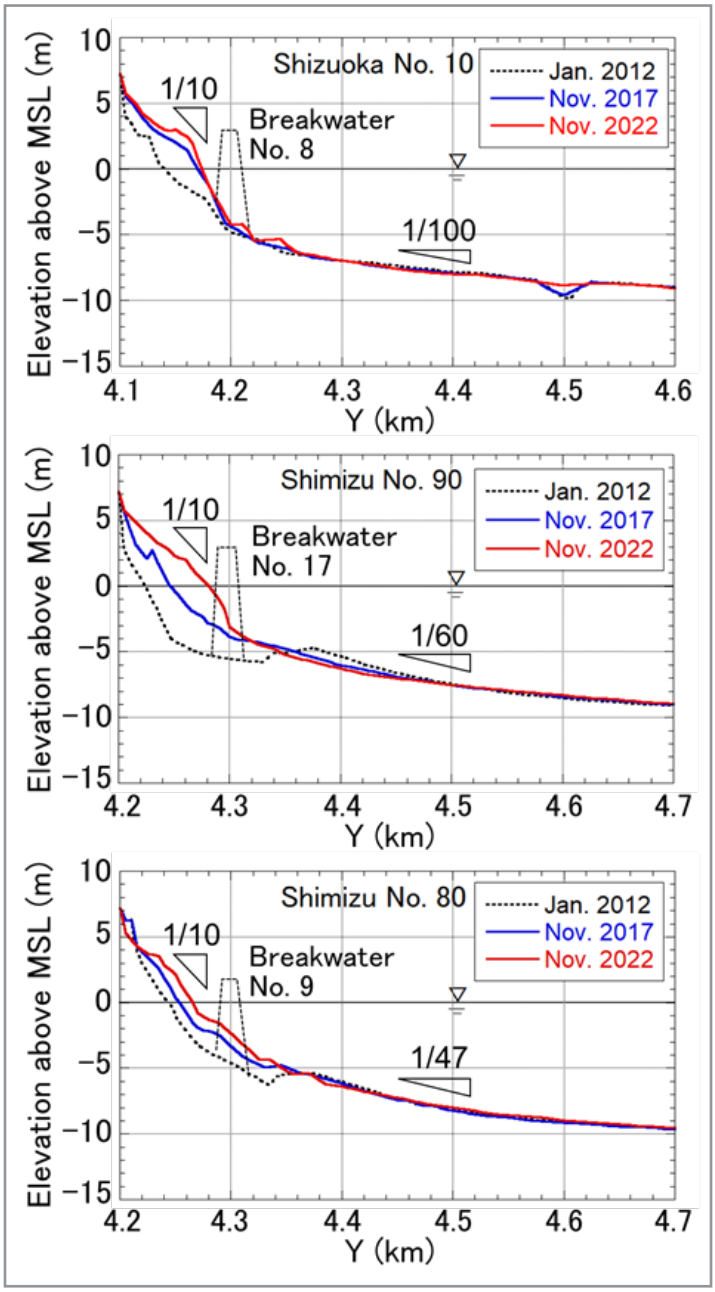

Figure 5: Changes in measured longitudinal profiles along three transects.

Figure 5 shows the changes in longitudinal profiles along typical three transects measured in 2012, 2017 and 2022 on these coasts, when adopting transects Shizuoka No. 10 and Shimizu Nos. 90 and 80, as shown in Fig. 4. Along Shizuoka No. 10 crossing detached breakwater No. 8, there exists a break in the slope at a depth of 4 m: a steep slope of 1/10 at a depth smaller than –4 m and a gentle slope of 1/100 offshore of –4 m depth. The topographic changes occur only at a depth smaller than –4 m and marked topographic changes can be seen near the shoreline, whereas topographic changes on the offshore slope are minimal. Furthermore, sand was deposited at a maximum thickness of 3.9 m behind the detached breakwater No. 8 until 2022, forming an upward convex profile.

Along Shimizu No. 90 crossing detached breakwater No. 17, local scouring was observed near the detached breakwater in 2012. Except for this, the longitudinal profile changes from 1/10 at a depth smaller than –4 m to a gentle slope of 1/60 on the offshore seabed, and the longitudinal slope breaks at a depth of –4 m with marked topographic changes at a depth smaller than –4 m. Along Shimizu No. 80, the seabed slope changes from 1/10 at a depth smaller than –4 m to a gentle slope of 1/47 in the offshore area with a break in the slope at a depth of –4 m. In addition, sand was deposited along this transect, resulting in the movement of the cross section in parallel in the cross-shore direction. Thus, on the Shizuoka and Shimizu coasts, beach changes have occurred owing to the movement of sand and gravel on a steep slope of approximately 1/10 at a depth smaller than –4 m under the con-

dition that a large number of detached breakwaters have been installed along the coastline [3].

Calculation Method

The wave field in the calculation domain, as shown in Fig. 2, was calculated by the energy balance equation method [8], and the topographic changes due to waves were calculated using the BG model [6, 7], given the distribution of the wave field. The wave field was calculated in a rectangular area of 13.5 km length alongshore and 7 km width in the cross-shore direction, whereas topographic changes were calculated in a rectangular area of 8.4 km length alongshore and 2.0 km width in the cross-shore direction included in the calculation domain of the wave field.

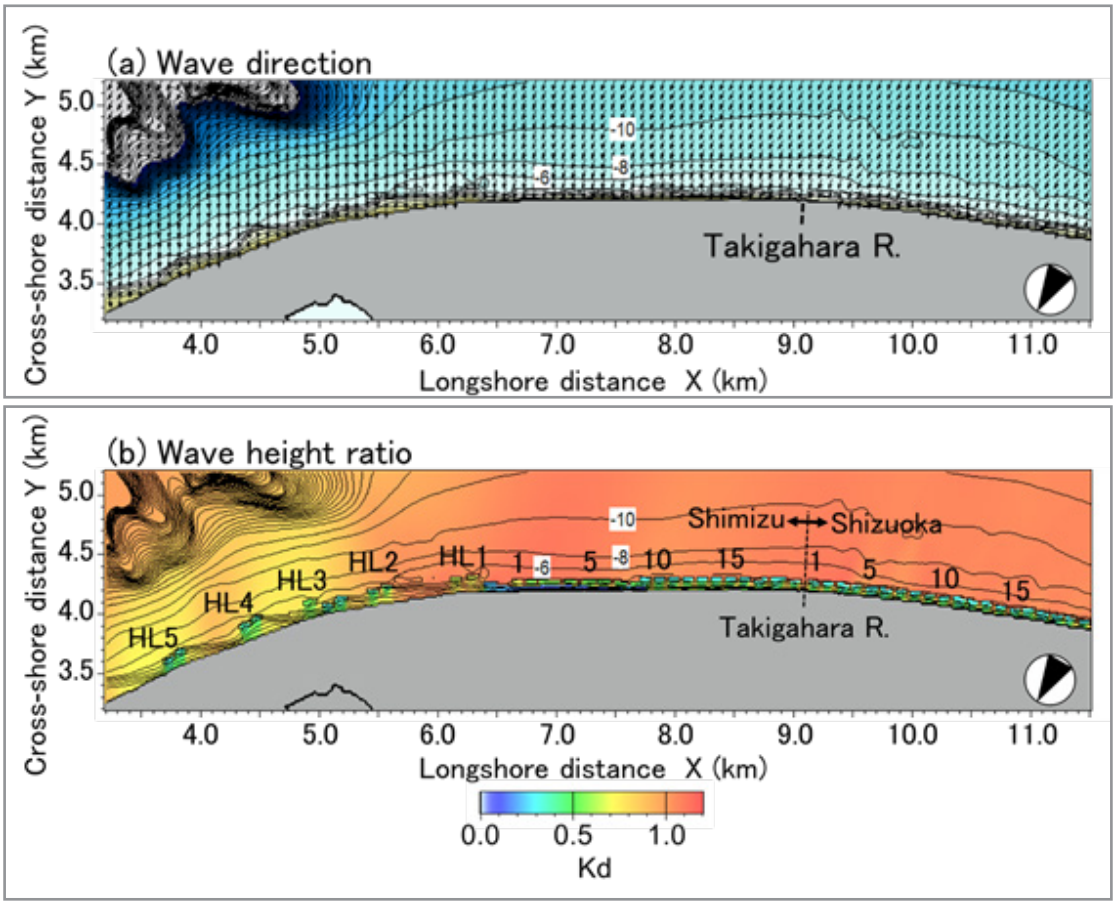

Figure 6: Distribution of wave direction and wave height ratio calculated using the wave energy balance equation [8].

As the incident wave conditions, a significant wave height of H = 3.3 m and a wave period of T = 9.0 s were adopted on the basis of wave observation results with an occurrence of probability of 5% measured at the Kuno wave observatory offshore of the Shizuoka coast to predict the averaged, long-term topographic changes. Although the predominant wave direction to the coast is approximately given by S, the wave field was calculated by trial and error at 5° intervals with reference to the wave angle of N180°, which rotated clockwise at an angle of 30° relative to the *Y*-axis, and then topographic changes were predicted. Finally, N175°E was selected as the best fit wave direction in reproducing the measured shoreline configuration, as shown in Fig. 6. When the wave field calculated using the energy balance equation was employed as it was, the shoreline significantly rotated counterclockwise downcoast of HL No. 5. Therefore, the wave direction in this area was locally corrected to enhance the accuracy of the reproduction calculation. For this purpose, the wave direction was corrected in the clockwise direction in a range from 0° to 5° between $X = 3.5$ and 3.4 km, and the wave angle was uniformly rotated clockwise by an angle of 5° between $X =$ 0 and 3.4 km.

As for the longitudinal profiles, the beach slope was assumed to be 1/10 at a depth smaller than –4 m, whereas a gentle slope of 1/50 extended –4 m offshore, as shown in Fig. 5. A close relationship exists between the grain size of bed materials and the seabed slope, so the steep slope of 1/10 between the land and –4 m depth was assumed to be composed of coarse sand and gravel, whereas the offshore seabed with a gentle slope of 1/50 was assumed to be composed of fine sand.

In the calculation of the topographic changes, the berm height h_R and the depth of closure h_c were determined to be 3 and 7 m, respectively, on the basis of the measured profiles, as shown in Fig. 5. The equilibrium slope tan β_c was determined to be 1/10 at a depth smaller than –4 m and 1/50 in a depth larger than –4

m. Because the beach material at a depth smaller than –4 m is composed of coarse sand and gravel, and the seabed at a depth larger than –4 m is covered with fine sand, the difference in the grain sizes was implicitly expressed by the change in $\tan\beta_c$.

The sediment transport rate was calculated to be the product of the wave energy flux multiplied by a coefficient of sediment transport, assuming that the beach changes occur proportionally to the depth distribution between h_R and $-h_c$. As shown in the change in longitudinal profiles in Fig. 5, marked beach changes only occurred at a depth shallower than –4 m. Therefore, a solid seabed was assumed at a depth deeper than –4 m.

The area bounded by X = 11.51 and 11.6 km was regarded as the entrance length for the calculation of the topographic changes, assuming the same cross section continues as that at X = 11.5 km. Regarding the downcoast boundary condition, a free boundary was set immediately upcoast of the L-shaped groin where the shoreline position was fixed. The seabed topography necessary for the calculation of the wave field was based on the results of the bathymetric survey in 2017 and the shoreline configuration determined from the aerial photographs taken in November 2017. Beach nourishment was carried out between 2012 and 2022 at a rate of 19,477 m^3/yr in area 1 between X = 8.0 and 8.88 km and at a rate of 76,750 m^3/yr in area 2 between X = 3.56 and 6.64 km, as shown in Fig. 4, and these volumes were artificially added as the sand volume per unit length along the shoreline.

The sand source was placed in front of the seawall such that the maximum beach elevations were 4 m in area 1 and 6.6 m in area 2 above the mean sea level. The duration of the reproduction calculation of beach changes was ten years from January 2012 to November 2022. The initial topography was given by the bathymetric data measured in January 2012.

Table 1: Calculation Conditions

Calculation model	Topographic changes: BG model [6, 7]
	Wave field: Energy balance equation of irregular waves [8]
Calculation domain	Wave field: 13.5 km alongshore and 7 km in cross-shore direction
	Topographic changes: 8.4 km alongshore and 2 km in the cross-shore direction
Calculation cases	Reproduction calculation from 2012 to the present
	Prediction calculation; Case 1 maintaining the present condition, Case 2 beach nourishment of 8×10^4 m^3/yr
Duration of calculation	Between January 2012 and November 2022 (reproduction)
	30 years from the present (prediction)
Initial bathymetry	Bathymetric map measured in January 2012 (reproduction)
	Reproduced bathymetry in 2022 (prediction)
Incident waves	H = 3.0 m, T = 9.0 s (waves with a probability of occurrence of 5%)
	Wave direction θ_w = N175°E (predominant wave direction)
Tide condition	M.S.L. ±0.0 m
Mesh size	$\Delta X = \Delta Y$ = 20 m
Time step	Δt = 5 h/step
Total steps	1,752 steps/yr
Equilibrium slope $\tan\beta_c$	1/10 between foreshore and -4 m, 1/50 deeper than -4 m
Critical slope of sinking of sand $\tan\beta_g$	$\tan\beta_g$ =1/2
Depth distribution of sand transport	Quadratic equation of the depth given by [9]
Depth of closure	h_c = 7 m
Berm height	h_R = 3 m
Coefficient of sand transport	Kx = 0.013, Ky/Kx = 1.0, K_2= 1.62 Kx [10]
Boundary conditions	Open boundary at right and left ends, no sand supply at offshore and landward ends
Beach nourishment (2012–2022)	Method of beach nourishment; formation of sand mound of 20 m width in front of the seawall
	Reproduction calculation; 19,477 m^3/yr between X = 8.0 and 8.88 km (total volume: 210,360 m^3), 76,750 m^3/yr between X = 3.56 and 6.64 km (828,000 m^3)
	Prediction calculation; leave as it is in Case 1, beach nourishment of 8×10^4 m^3/yr between X =3.56 and 6.64 km in Case 2.
Wave transmission coefficient	0.3 (Shizuoka detached breakwaters), 0.6 (Shimizu No. 1), 0.5 (Shimizu Nos. 2–8), 0.3 (Shimizu Nos. 9–13), 0.2 (breakwater at shoreline), 0.6 (HL1), 0.4 (HLs 2 and 3), 0.5 (HLs 4 and 5)

Because a large number of detached breakwaters have been constructed along these coasts, the wave dissipating effect of these breakwaters was evaluated using different wave transmission coefficients: 0.3 for the detached breakwaters on the Shizuoka coast, 0.6 for Shimizu No. 1, and 0.5 for Shimizu Nos. 2–8, and 0.3 for Shimizu Nos. 9–19. In addition, the breakwaters have been installed along the shoreline behind Shimizu Nos. 1–8, and therefore, the wave transmission coefficient of these breakwaters was assumed to be 0.7. Table 1 shows the calculation conditions.

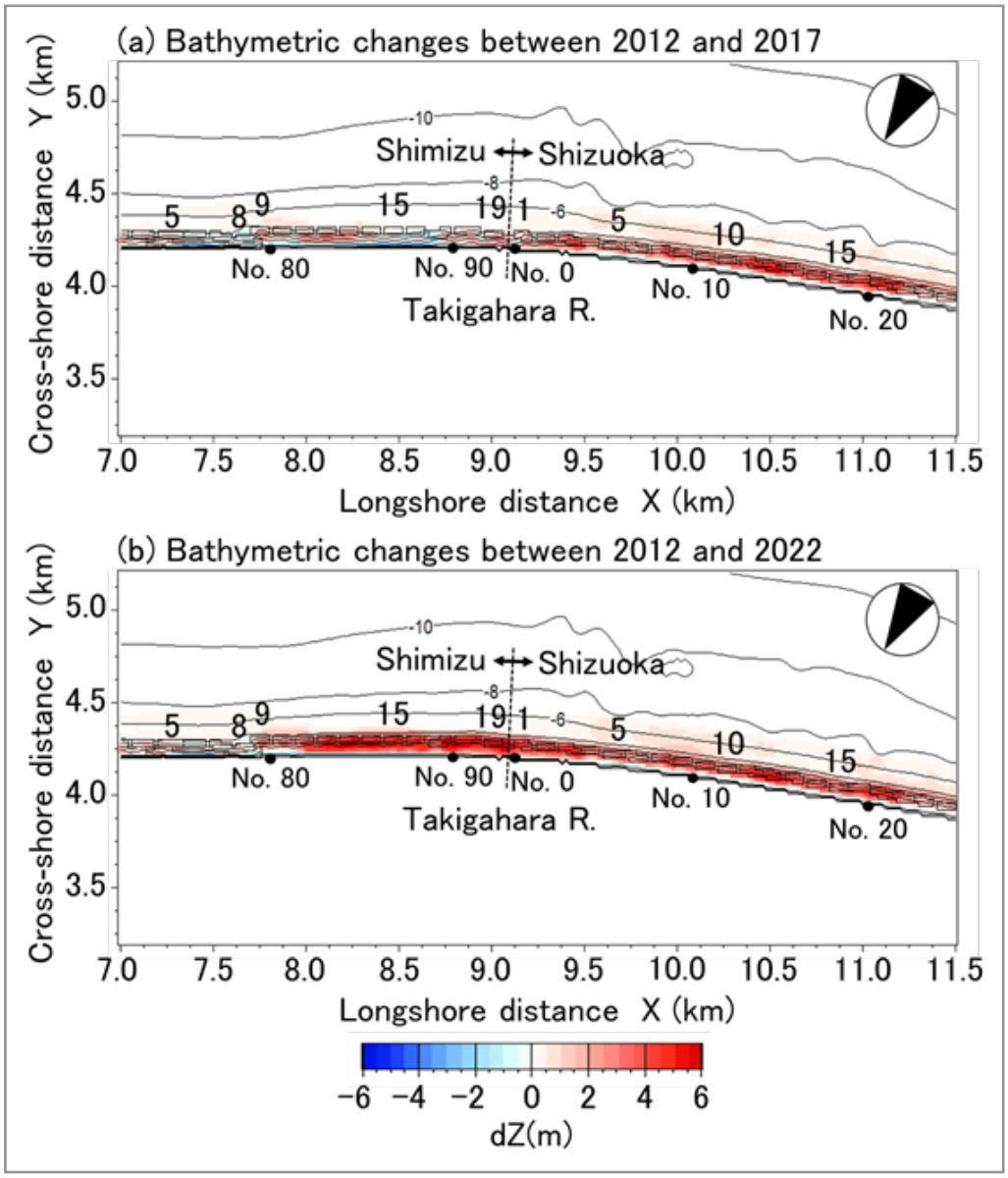

Figure 7: Topographic changes until 2017 and 2022 with reference to that in 2012.

Results of Reproduction Calculation

The topographic changes until 2017 and 2022 relative to that in 2012 are shown in Fig. 7. Although the sand body where marked sand deposition occurs was located at the east end of the Shizuoka coast in 2017, it reached the location of detached breakwater Shimizu No. 9 in 2022.

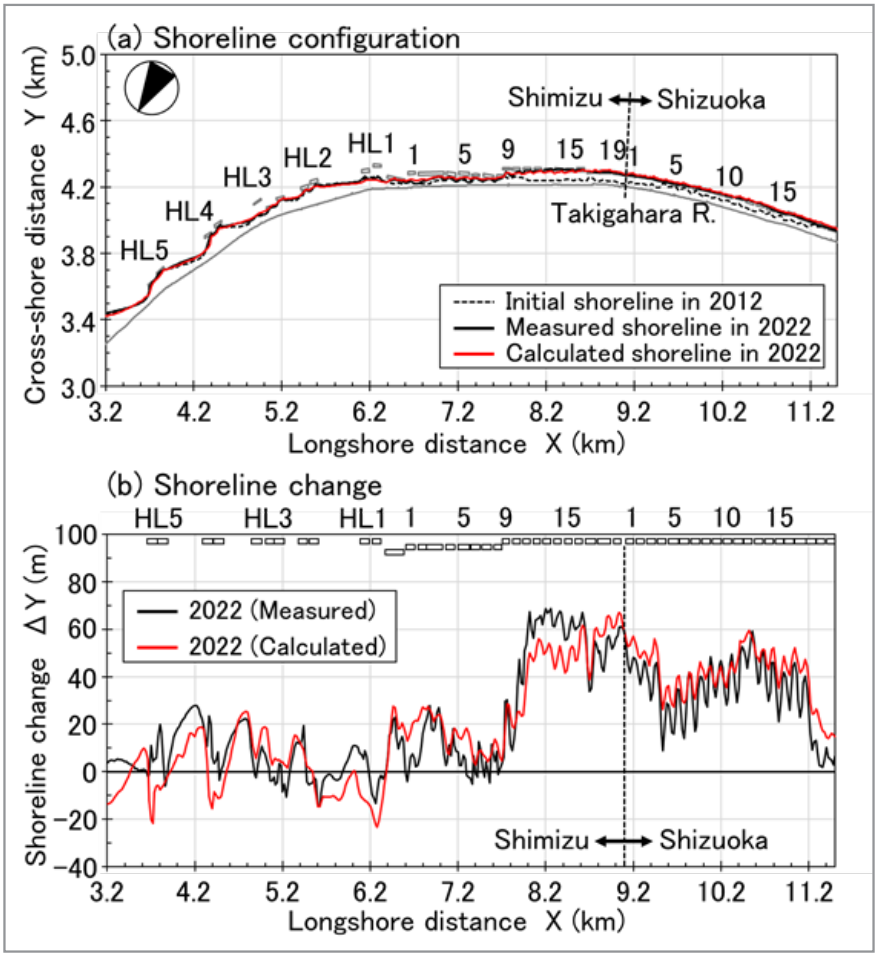

Figure 8: Comparison of measured and calculated shoreline configurations until 2022.

Figure 8(a) shows the measured and calculated shoreline configurations in 2022. Although the shoreline was not attached to the detached breakwaters near the west end in 2012, sand was deposited up to behind Shimizu No. 9 and the shoreline connected to the detached breakwater in 2022. However, the shoreline did not change compared with that in 2012 northeast of Shimizu No. 9 because the sand body did not reach there. Figure 8(b) shows the measured and calculated shoreline changes from 2012 to 2022 with the location of detached breakwaters in this area. The calculated and measured shoreline changes are in good agreement in the sense that the embayment shoreline was formed at the opening between the detached breakwaters, whereas the shoreline advanced behind the detached breakwaters forming cuspate forelands in the entire area between the Shizuoka coast and Shimizu No. 9. In contrast, the shoreline advance was minimal in the area where the offshore distance of the detached breakwater was as small as 40–60 m northeast of Shimizu No. 9 since the sand body had not arrived there until 2022. In addition, the spiked shoreline recession behind the artificial headland was also reproduced well.

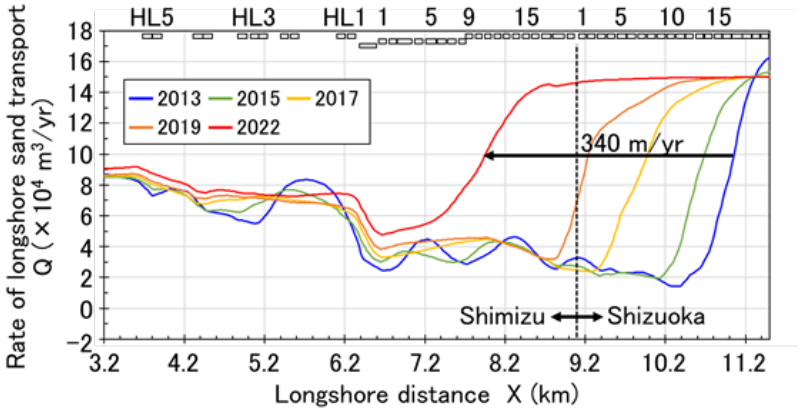

Figure 9: Change in longshore sand transport until 2022.

Figure 9 shows the distribution of the rate of longshore sand transport. In this calculation, the updrift end had an open boundary for longshore sand transport, where approximately 1.5×10^5 m^3/yr was supplied in response to the wave conditions. This longshore sand transport approximately corresponds to the longshore sand transport of 1.3×10^5 m^3/yr obtained from the analysis of bathymetric data [3]. Detached breakwaters of Shizuoka Nos. 1–20 and Shimizu Nos. 9–19 have been continuously constructed in parallel to the coastline with the wave transmission coefficient K_t of 0.3, and longshore sand transport was reduced alongshore because of the wave dissipation effect of these detached breakwaters. As sand was fully deposited behind the detached breakwaters, the area with a marked reduction in longshore sand transport propagated at a velocity of 340 m/yr over time.

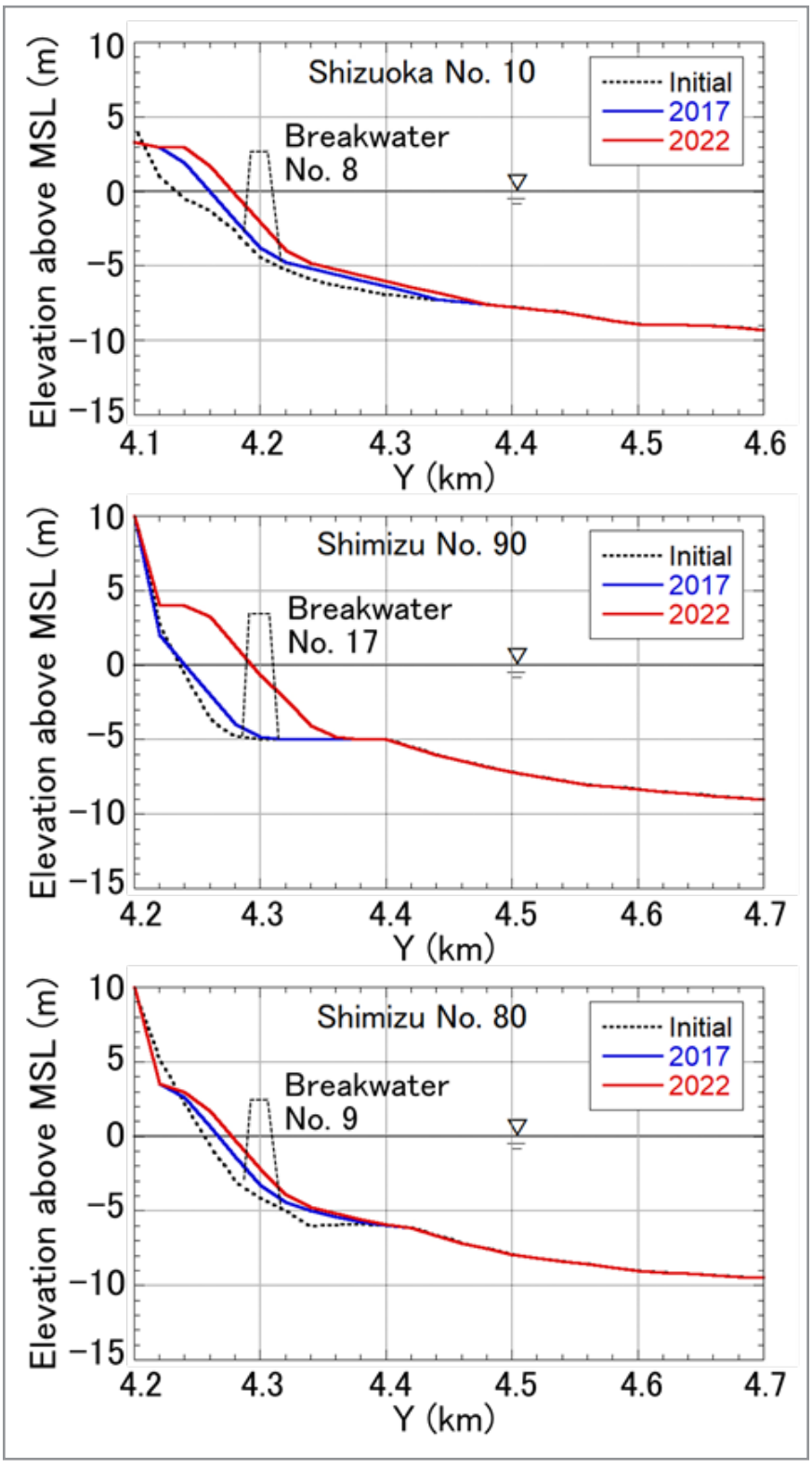

Figure 10: Calculated longitudinal profile along transect Shizuoka No. 10 and Shimizu Nos. 90 and 80.

Figure 10 shows the calculated longitudinal profiles along three transects, which correspond to the measured longitudinal profiles shown in Fig. 5. Along Shizuoka No. 10, the accretion at a depth between –5 and +3 m behind breakwater No. 8 was well reproduced. Along Shimizu No. 90, although sand deposition was slightly overestimated, the overall deposition of sand behind the detached breakwater was reproduced. Along the transect Shimizu No. 80, the amount of sand deposited was small, but overall profile changes were reproduced. Thus, the changes in longitudinal profiles were well reproduced by the present model [6, 7].

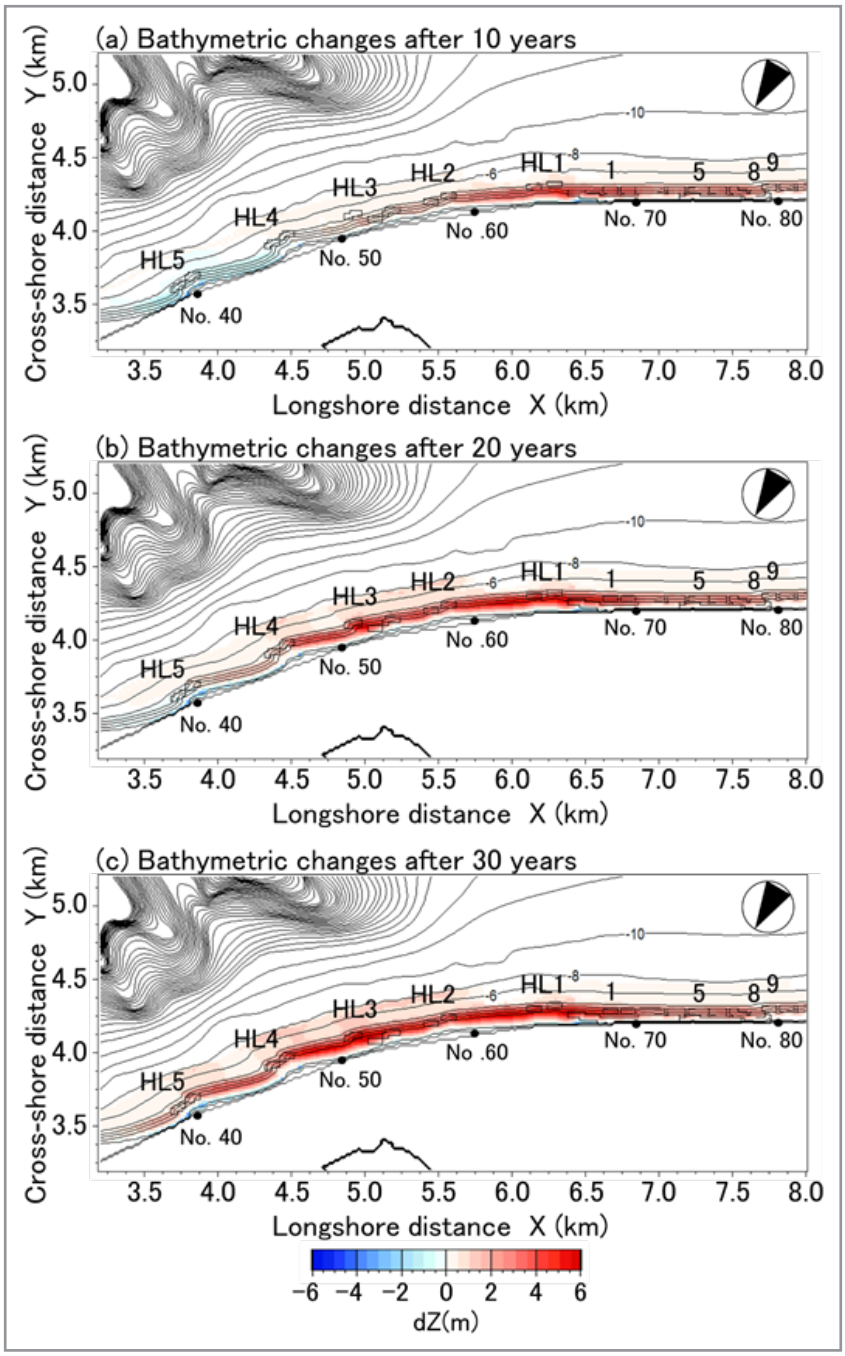

Figure 11: Topographic changes 10, 20 and 30 years from the present (Case 1).

Prediction Results

Since the reproduction calculation using the BG model in an extensive area of the Shizuoka and Shimizu coasts became possible, the topographic changes in the northeast part of the Shimizu coast including the area where artificial headlands have been installed were predicted using the present model, as well as the study on the effect of the beach nourishment. Calculations for two cases were carried out: the beach changes over 30 years from the present without beach nourishment under the present condition (Case 1), and the prediction of beach changes with the given beach nourishment of 8×10^4 m^3/yr between X = 3.56 and 6.64 km (Case 2). In both cases, the results of the numerical

simulation until November 2022 were employed as the initial topography.

The topographic changes in Case 1 10, 20 and 30 years from the present are shown in Fig. 11. Sand transported by littoral drift from the southwest part of the coast will be fully deposited along the shoreline up to the location of HL2 while burying the detached breakwaters 10 years from the present. Furthermore, sand will be deposited alongshore up to the location of HL4 after 20 years and HL5 after 30 years.

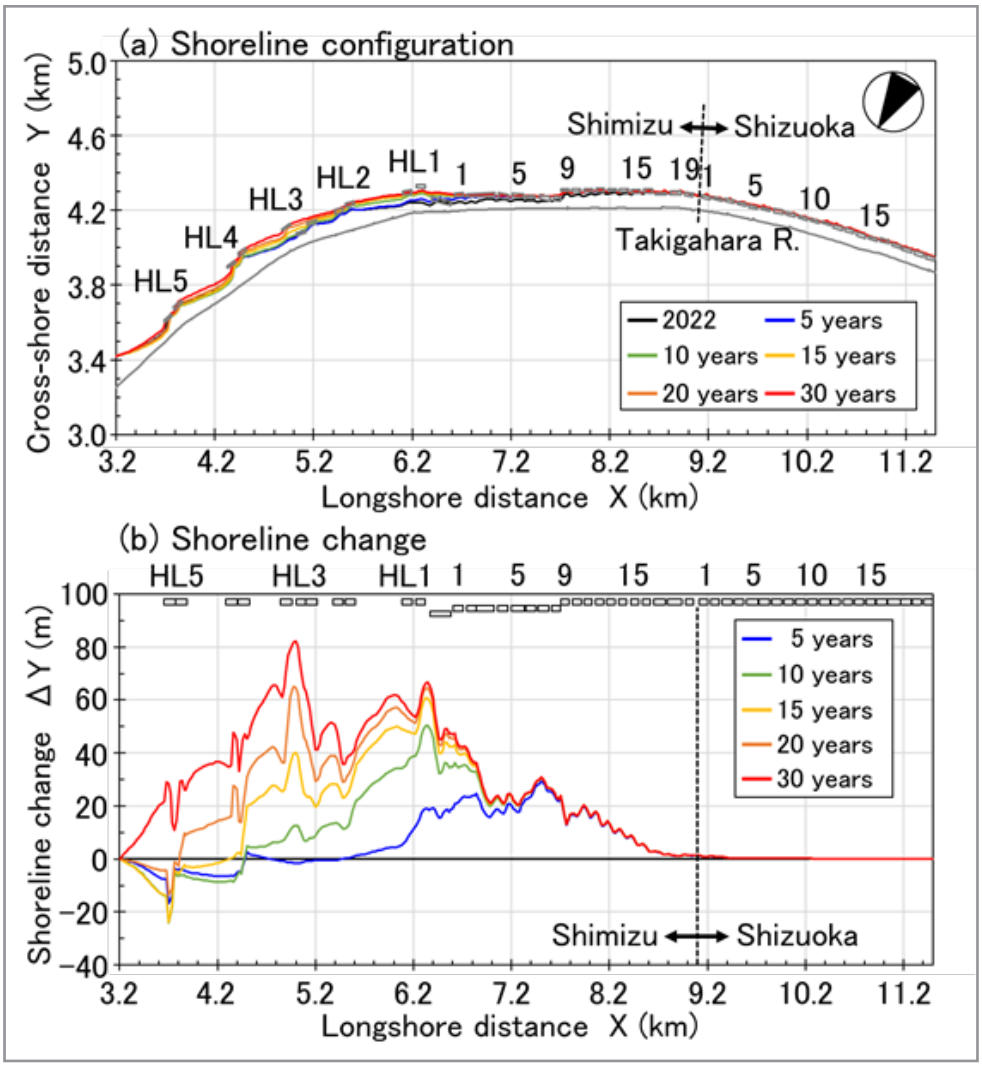

Figure 12: Shoreline configuration and shoreline changes over 30 years (Case 1).

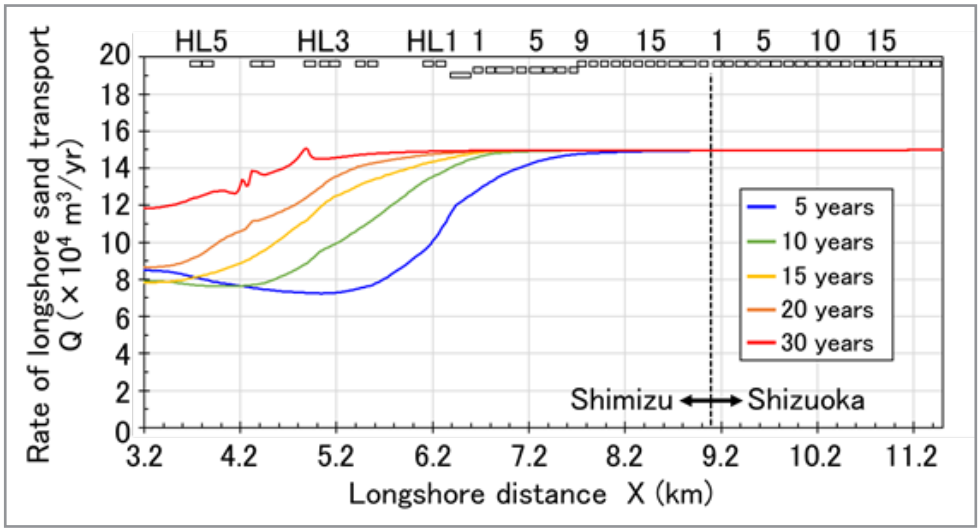

Figure 13: Distribution of longshore sand transport (Case 1).

Although sand will be deposited in the northeast part of the Shimizu coast by the northeastward longshore sand transport, 30 years will be needed for the sand accumulation zone to reach HL5. Figure 12 shows the shoreline configuration and shoreline changes during this period. Because approximately 1.5×10^5 m³/yr of sand was supplied from the upcoast, sand was deposited in the vicinity of Shimizu Nos. 1–8, and the shoreline advanced up to the offshore side of the detached breakwaters. Then, the shoreline markedly advanced around the area protected by HLs. Figure 13 shows the distribution of the longshore sand transport rate. The rapid-reduction area in longshore sand transport moved northeastward over time. Although the rate of longshore sand transport at the left boundary is approximately 8×10^4 m³/yr 10 years from now, it will increase to up to 1.2×10^5 m³/yr after 30 years, resulting in the increase in sediment supply by 50% to the north end of the sand spit.

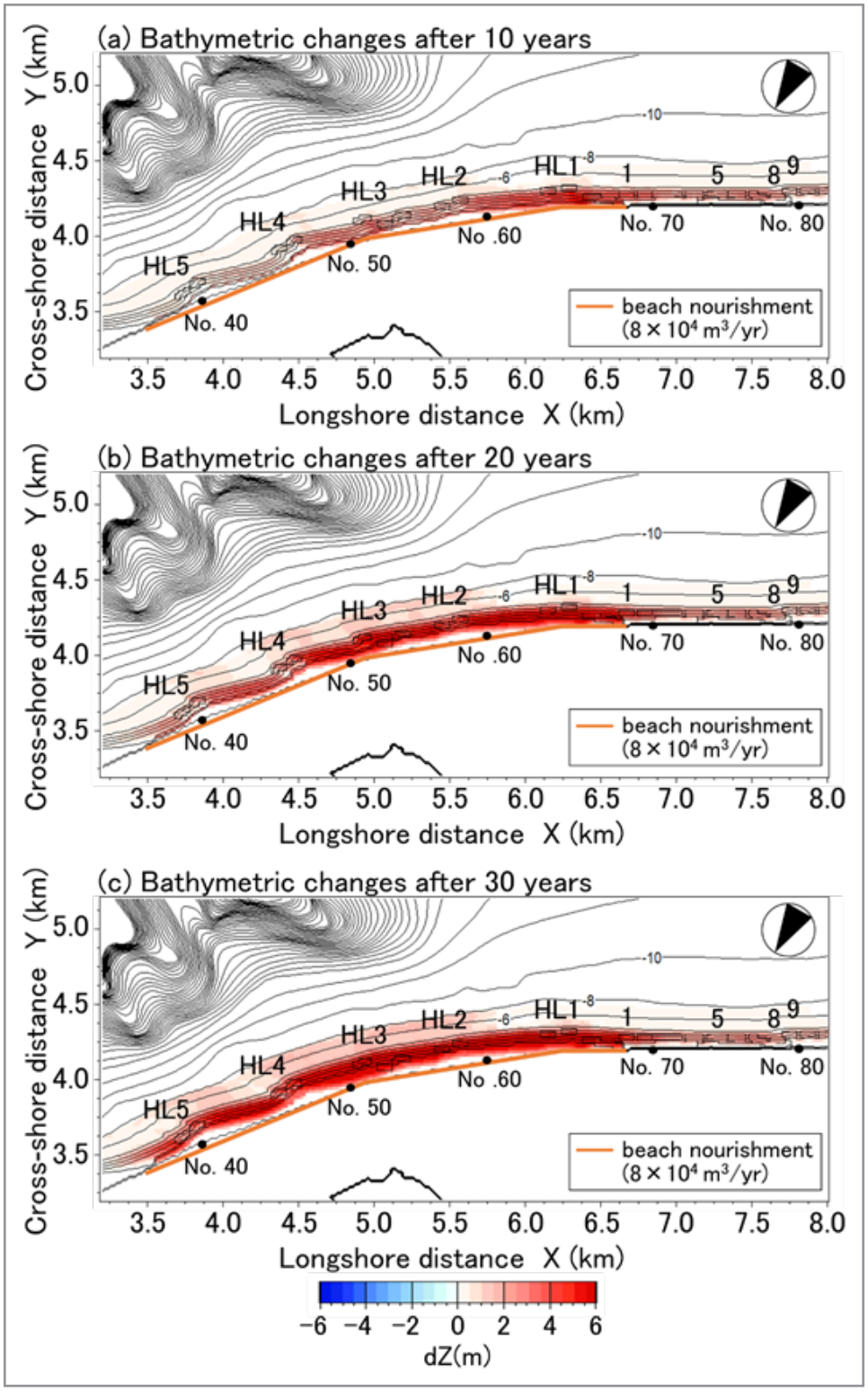

Figure 14: Topographic changes 10, 20 and 30 years from the present (Case 2).

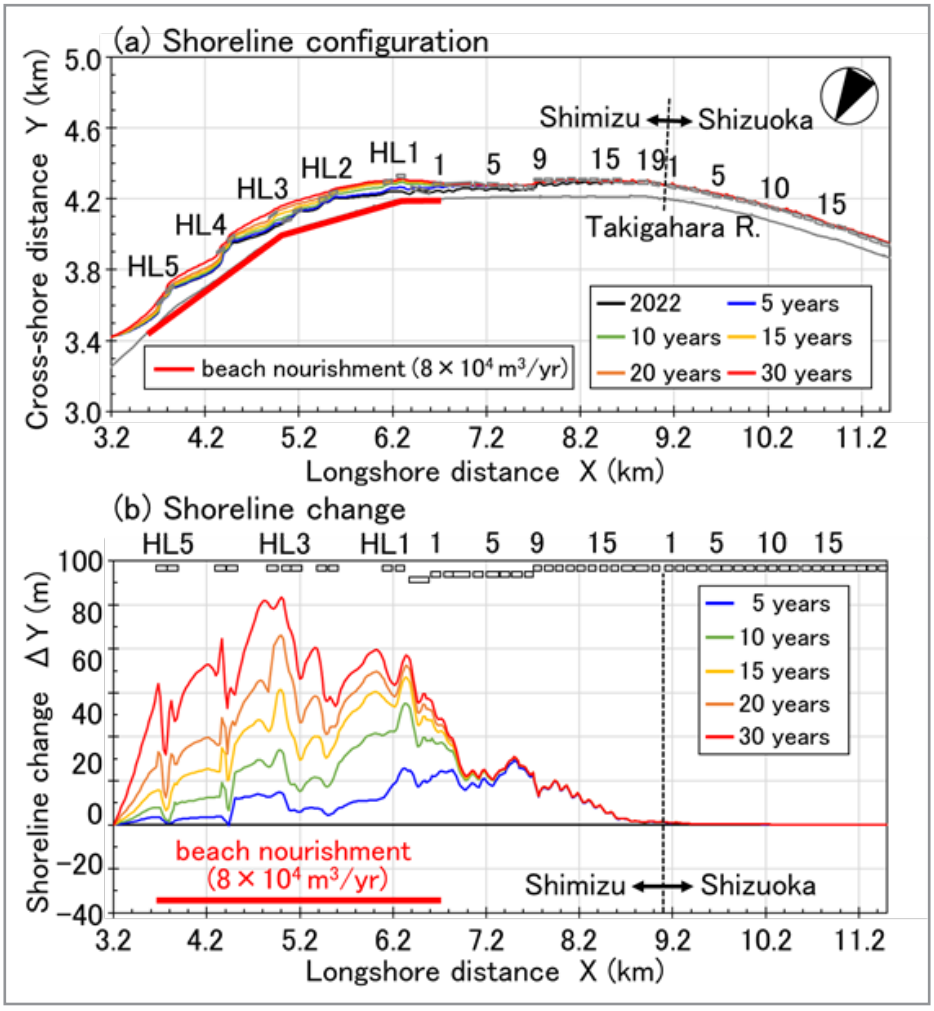

Figure 15: Shoreline configuration and shoreline changes over 30 years (Case 2).

In Case 2, beach nourishment was carried out at a rate of 8×10^4 m^3/yr between $X = 3.56$ and 6.64 km. Figures 14 and 15 show the topographic changes 10, 20 and 30 years from the present and the shoreline configuration and shoreline changes over 30 years, respectively. After 10 years, the sand body will arrive at HL2, the movement of which was caused by natural longshore sand transport and beach nourishment at a rate of 8×10^4 m^3/yr. Furthermore, the sand body arrived at HL4 and HL5 after 20 and 30 years, respectively, resulting in a marked increase in the beach width. Thus, the beach nourishment of 8×10^4 m^3/yr is very much effective for the recovery of the sandy beach for HL1–HL4 to be buried by sand.

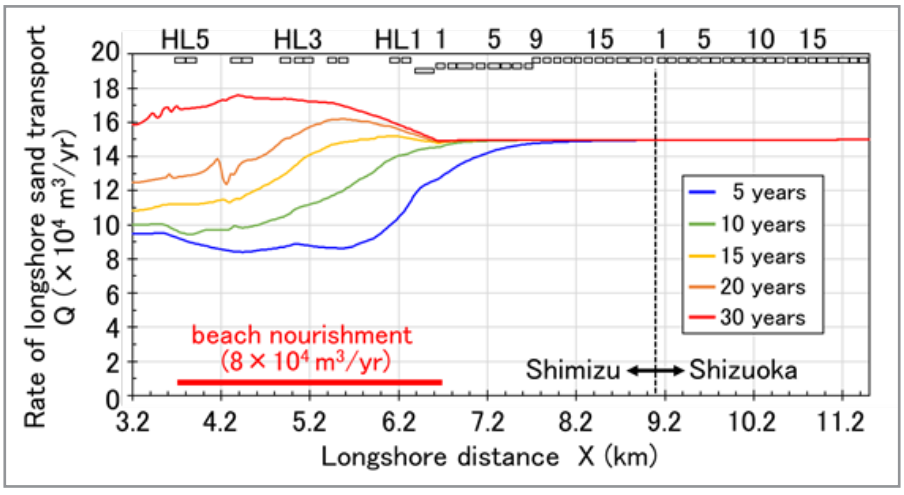

Figure 16: Distribution of longshore sand transport (Case 2).

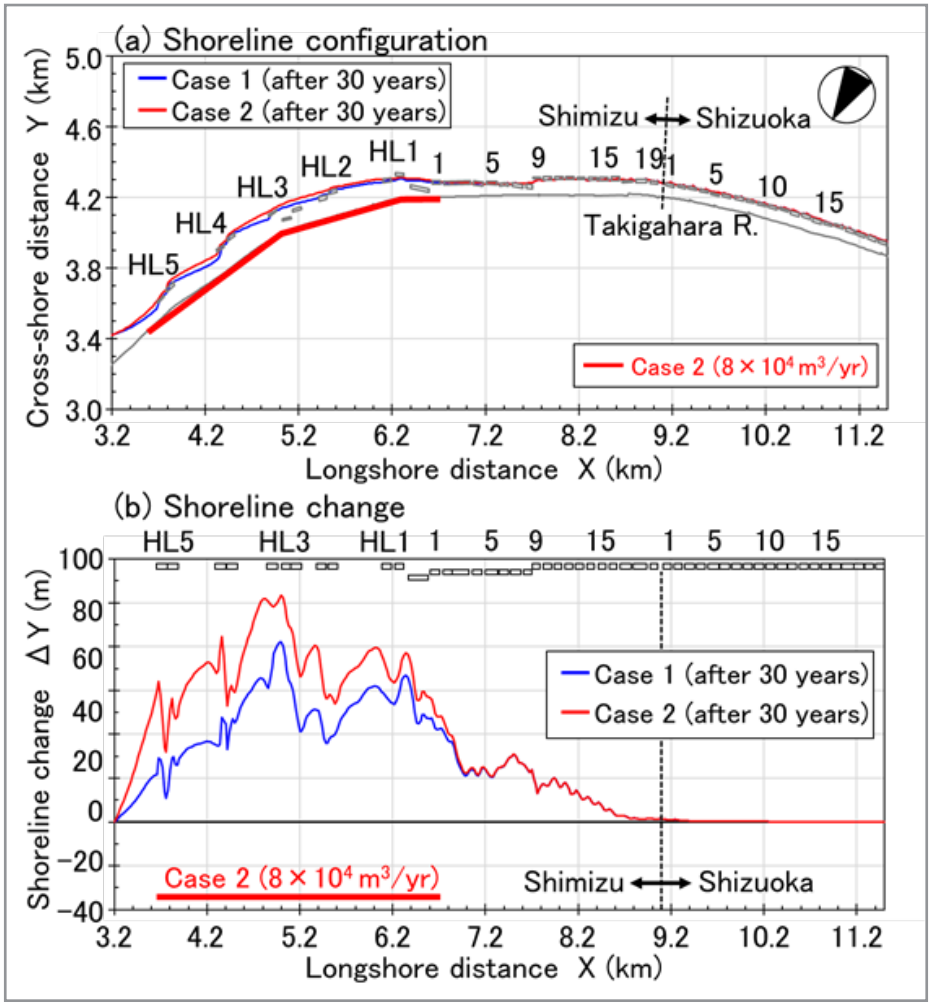

Figure 17: Comparison of shoreline configuration and shoreline change over 30 years (Case 1 vs Case 2).

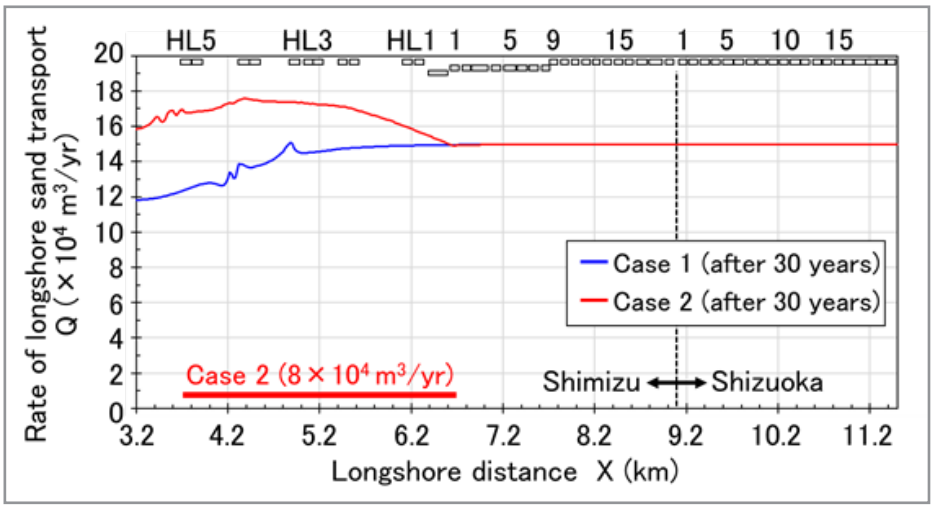

Figure 18: Comparison of distribution of longshore sand transport over 30 years (Case 1 vs Case 2).

Figure 16 shows the distribution of longshore sand transport over 30 years. The area where the longshore sand transport rapidly decreases alongshore will move eastward over time, resulting in the increase in sand transport at the east end of the calculation domain from 1.0×10^5 m^3/yr after 10 years and 1.6×10^5 m^3/yr after 30 years. Figures 17 and 18 show the comparison of Cases 1 and 2 with respect to the shoreline configuration and shoreline changes, and longshore sand transport, respectively, over 30 years. The longshore sand transport at the northeast end of the calculation domain increased from 1.2×10^5 m^3/yr in Case

1 to 1.6×10^5 m^3/yr in Case 2, which is effective for reducing the volume of sand back pass of 5×10^4 m^3/yr from the tip of the sand spit, which has been continuously carried out to maintain the shoreline downcoast of HL5.

Conclusion

The movement of the sand body along the Shizuoka and Shimizu coasts between 2012 and 2022 was investigated using the BG model (a model for predicting 3-D beach changes based on Bagnold's concept). By this calculation, we were able to well reproduced overall beach changes associated with the movement of the sand body. Also, the effect of beach nourishment to enhance the velocity of the sand body to the tip of the sand spit was predicted. It was confirmed that beach nourishment at a rate of 8×10^4 m^3/yr is required to maintain or recover a sandy beach on the Shimizu coast.

References

1. Uda, T., Yamamoto, Y., Itabashi, N., & Yamaji, K. (1996). Field observation of movement of sand body due to waves and verification of its mechanism by numerical model. In Proceedings of the 25th International Conference on Coast al Engineering (ICCE), 137–150.
2. Uda, T., Nishitani, M., Serizawa, M., San-nami, T., & Ishi kawa, T. (2007). Numerical analysis of movement of sand body using a contour-line-change model. Transactions of the Japanese Geomorphological Union, 28(4), 399–414.
3. Uda, T. (2017). Japan's beach erosion: Reality and future measures (2nd ed., p. 530). World Scientific.
4. Uda, T., Serizawa, M., Nishitani, M., & Ishikawa, T. (2008). Field investigation and numerical simulation of movement of sand body. In Proceedings of the 31st International Con ference on Coastal Engineering (ICCE), 2051–2063.
5. San-nami, T., Uda, T., Ohashi, N., Iwamoto, H., Seriza wa, M., Ishikawa, T., & Miyahara, S. (2012). Prediction of beach erosion caused by reduction of fluvial sand supply due to excess sand mining and beach recovery after prohi bition of mining. In Proceedings of the 33rd International Conference on Coastal Engineering (ICCE), sediment.61, 1–11.
6. Serizawa, M., Uda, T., San-nami, T., & Furuike, K. (2006). A model for predicting beach changes based on Bagnold's concept. Journal of the Japan Society of Civil Engineers, Series B, 62(4), 330–347.
7. Uda, T., Serizawa, M., & Miyahara, S. (2018). Morpho dynamic model for predicting beach changes based on Bagnold's concept and its applications (p. 188). INTECH. https://www.intechopen.com/books/morphodynamic-mod el-for-predicting-beach-changes-based-on-bagnold-s-con cept-and-its-applications.
8. Mase, H., Takayama, T., Kunitomi, S., & Mishima, T. (1999). Multi-directional spectral wave transformation model including diffraction effect. Journal of the Japan So ciety of Civil Engineers, (628/I148), 177–187.
9. Uda, T., & Kawano, S. (1996). Development of contour line-change model for predicting beach changes. Journal of the Japan Society of Civil Engineers, (539/II35), 121–139.
10. Ozasa, H., & Brampton, A. H. (1980). Model for predict ing the shoreline evolution of beaches backed by seawalls. Coastal Engineering, 4, 47–64.